

## COSMOLOGICAL PARAMETER CONSTRAINTS FROM CMB LENSING WITH COSMIC VOIDS

TEERAPARB CHANTAVAT<sup>1,2†</sup>, UTANE SAWANGWIT<sup>3</sup>, P. M. SUTTER<sup>4,5,6</sup>, AND BENJAMIN D. WANDELT<sup>4,5,7</sup>(Dated: January 27, 2023)  
Draft version January 27, 2023

## ABSTRACT

We investigate the potential of using cosmic voids to constrain cosmological parameters through gravitational lensing of the cosmic microwave background (CMB) and make predictions for the next generation surveys. By assuming the detection of a series of  $\approx 10$  voids of size  $R_V \gtrsim 20 \text{ Mpc } h^{-1}$  along a line of sight with  $\approx 100 - 200$  independent square-degree patches of the sky, we could potentially get constraints of cosmological parameter that are competitive with PLANCK alone. The chance of finding such patches are seemingly small but given the fact that voids occupy the vast majority of volume of the universe, finding a few of those patches and combining them to get constraints on cosmological parameters is possible. This analysis is based on our current knowledge of the average void profile and analytical estimates of the void number function in upcoming surveys. The full potential of this technique relies on an accurate determination of the void profile to  $\approx 10$  percent level. CMB lensing with voids will provide a competitive and complimentary route to parameter constraints for the next generation cosmological observations. For example, we predict that for a EUCLID-like mission the constraints are  $100\omega_b = 2.26 \pm 0.05$ ,  $\omega_c = 0.114 \pm 0.004$ ,  $\Omega_\Lambda = 0.684 \pm 0.014$ ,  $\Delta_R^2 = (2.40 \pm 11.05) \times 10^{-9}$ ,  $n_s = 0.971 \pm 0.026$ ,  $\tau = 0.0851 \pm 2.4947$  for our conservative prediction with 100 square-degree patches.

**Keywords:** cosmic background radiation — cosmological parameters — gravitational lensing: weak — large-scale structure of universe

## 1. INTRODUCTION

Observations of the cosmic microwave background (CMB) of the Universe have provided a wealth of information about the initial conditions and the structure of our early Universe (for a recent review see [Aghanim et al. 2008](#)). Recent observations of the CMB ([Hinshaw et al. 2013](#); [Planck Collaboration 2013a](#)) have shown that our Universe is highly Gaussian with nearly scale-invariant power spectrum. This has provided our picture of the Universe as the standard model called the inflationary  $\Lambda$ CDM model ([Carroll et al. 1992](#)).

In the  $\Lambda$ CDM model, the Universe is homogeneous and isotropic on large scales. However, on small scales, the hierarchical clustering of matter leads to formations of complex cosmic structure such as clusters of galaxies, walls, filaments and voids ([Boylan-Kolchin et al. 2009](#)). Among these objects, voids occupy a vast majority of space and hence provide the largest volume-based test on theories of structure formation ([Biswas et al. 2008](#); [Bos et al. 2008](#)). Recently cosmic voids are being continually found amounting to releases of public void catalogues ([Pan et al. 2012](#); [Sutter et al. 2012a, 2014c](#)).

The CMB signal from the surface of last scattering has traversed the Universe for 13.8 billion years to reach us, passing through intervening clusters and voids along the line of

sight. The trajectories of CMB photons are bent towards gravitating matter due to distortion of spacetime caused by gravitational lensing ([Blanchard & Schneider 1987](#)). The gravitational lensing sources distort the CMB temperatures giving rise to the transfer of CMB angular power spectrum to smaller scales ([Smith et al. 2006](#)). The secondary anisotropies due to lensing effects add cosmological information on the growth of structure and local curvature of the Universe. The scenario is reversed when voids are acting as the sources of gravitational lenses. The de-lensing effect of voids has been investigated and recently observed through the distortions of background galaxies by a stacking method which enhances the signal ([Higuchi et al. 2013](#); [Krause et al. 2013](#); [Melchior et al. 2014](#)). The integrated Sachs-Wolfe effect by voids has also been investigated and detected ([Cai et al. 2014](#); [Ilić et al. 2013](#); [Planck Collaboration 2013b](#)). A precision cosmology with void is also attainable – the Alcock-Paczynski test could be applied to the morphology of stacked void in order to infer the underlying cosmology with good precisions ([Lavaux & Wandelt 2012](#); [Sutter et al. 2012b](#)).

The goal of this *article* is to investigate the potential of utilising voids as probes of cosmology by observing the lensing effect of the CMB, and understand the requirements for the detectability of the effect for the next generation surveys such as BigBOSS ([BigBOSS Collaboration 2009](#)), DES ([DES Collaboration 2006](#)), LSST ([LSST Science Collaboration 2009](#)) and EUCLID ([Laureijs et al. 2011](#)). Throughout this *article*, our fiducial cosmological parameters for Fisher analysis are  $\{100\omega_b, \omega_c, \Omega_\Lambda, \Delta_R^2, n_s, \tau\} = \{2.20, 0.120, 0.682, 2.22 \times 10^{-9}, 0.962, 0.0925\}$ , which is consistent with PLANCK + WMAP Paralization maximum likelihood cosmological parameters ([Planck Collaboration 2013a](#)) with  $w = -1$  and  $\Omega_k = 0$  as the standard flat  $\Lambda$ CDM cosmology. The matter power spectrum and the angular power spectrum were computed using CAMB<sup>8</sup> ([Lewis et al. 2000](#)).

<sup>†</sup> E-mail: teeraparb@nu.ac.th

<sup>1</sup> ThEP's Laboratory of Cosmology and Gravity, The Institute for Fundamental Study, Naresuan University, Phitsanulok 65000, Thailand

<sup>2</sup> Thailand Center of Excellence in Physics, Ministry of Education, Bangkok 10400, Thailand

<sup>3</sup> National Astronomical Research Institute of Thailand (NARIT), Chiang Mai, 50200, Thailand

<sup>4</sup> UPMC Univ Paris 06, UMR7095, Institut d'Astrophysique de Paris, F-75014, Paris, France

<sup>5</sup> CNRS, UMR7095, Institut d'Astrophysique de Paris, F-75014, Paris, France

<sup>6</sup> Center for Cosmology and Astro-Particle Physics, the Ohio State University, Columbus, Ohio 43210, USA

<sup>7</sup> Department of Astronomy, University of Illinois at Urbana-Champaign, Urbana, IL 61801, USA

<sup>8</sup> <http://camb.info>

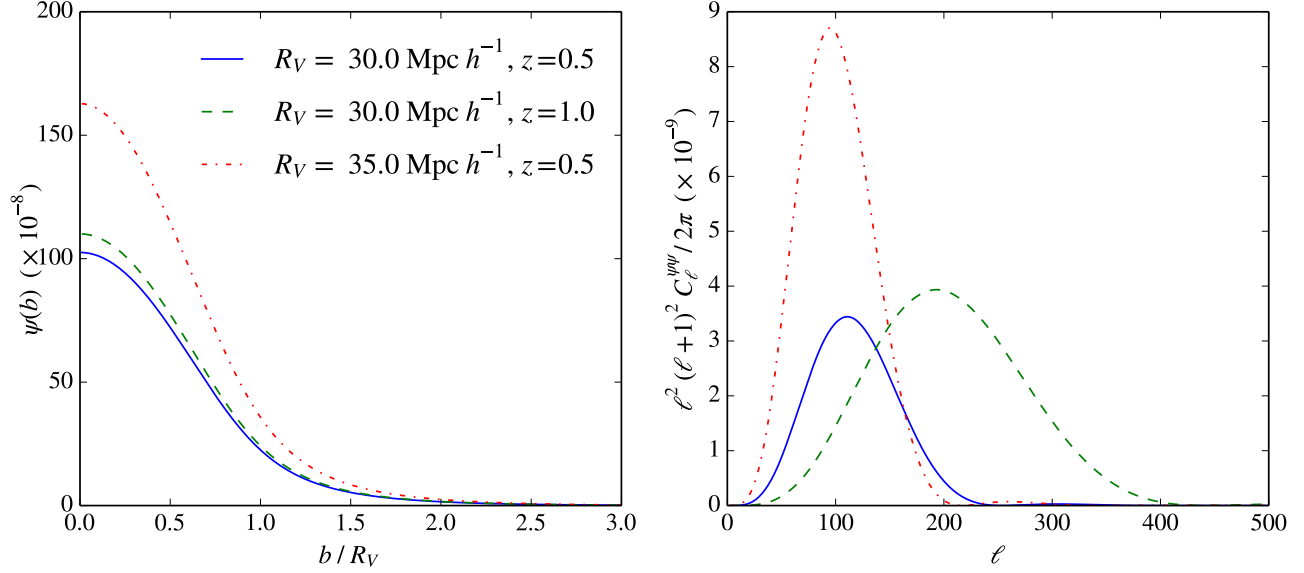


**Figure 1.** The lensing potentials of a single void in real space as a function of impact parameter  $b$  (left) and their corresponding angular power spectra (right) for voids with  $R_V = 30.0 \text{ Mpc } h^{-1}$  at  $z = 0.5$  (solid),  $R_V = 30.0 \text{ Mpc } h^{-1}$  at  $z = 1.0$  (dashed) and  $R_V = 35.0 \text{ Mpc } h^{-1}$  at  $z = 0.5$  (dot-dashed).

## 2. THEORY

The formalism for CMB lensing correlations, covariance and Fisher information matrices is given in the context of the flat-sky approximation which is appropriate for small scale CMB lensing (Hu 2000). We advise readers to consult Lewis & Challinor (2006) for a complete and rigorous review of recent advancements on the theory of CMB lensing and Bartelmann & Schneider (2001) for a general review of gravitational weak lensing.

### 2.1. CMB Lensing - Flat sky approximation

We consider a lensed CMB temperature anisotropy in the direction  $\hat{n}$  on the sky,  $\tilde{\Theta}(\hat{n})$ , and an unlensed temperature anisotropy  $\Theta(\hat{n} + \alpha)$  where  $\alpha$  is the deflection angle due to a source with lensing potential  $\psi(\hat{n})$ ,  $\alpha \equiv \nabla\psi(\hat{n})$ .  $\tilde{\Theta}(\hat{n})$  can be expanded as

$$\begin{aligned} \tilde{\Theta}(\hat{n}) &= \Theta(\hat{n}) + \nabla_i \psi \nabla^i \Theta(\hat{n}) \\ &\quad + \frac{1}{2} \nabla_i \psi \nabla_j \psi \nabla^i \nabla^j \Theta(\hat{n}) + O(\psi^3). \end{aligned} \quad (1)$$

The Fourier transform of Eq. (1) is

$$\tilde{\Theta}(\ell) = \Theta(\ell) - \int \frac{d^2 \ell_1}{(2\pi)^2} \Theta(\ell_1) L(\ell, \ell_1), \quad (2)$$

where the lensing kernel  $L(\ell, \ell_1)$  is given by

$$\begin{aligned} L(\ell, \ell_1) &= \psi(\ell - \ell_1)(\ell - \ell_1) \cdot \ell_1 \\ &\quad - \frac{1}{2} \int \frac{d^2 \ell_2}{(2\pi)^2} \psi(\ell_2) \psi(\ell - \ell_1 - \ell_2)(\ell_1 \cdot \ell_2) \\ &\quad \times (\ell_1 \cdot (\ell - \ell_1 - \ell_2)). \end{aligned} \quad (3)$$

$\Theta(\hat{n})$  is assumed Gaussianly distributed. Therefore, the only independent correlation function is the two-point correlation function,

$$\langle \Theta(\ell)^* \Theta(\ell') \rangle = (2\pi)^2 \delta_D^2(\ell - \ell') C_\ell^{\Theta\Theta}, \quad (4)$$

where  $\delta_D^2(\ell - \ell')$  is the 2D Dirac's delta function and  $C_\ell^{\Theta\Theta}$  is the  $\Theta\Theta$ -multipole moment of the order  $\ell$ . From Eqs. (2) - (4),

$$\begin{aligned} \tilde{C}_\ell^{\Theta\Theta} &= C_\ell^{\Theta\Theta} \left[ 1 - \int \frac{d^2 \ell_1}{(2\pi)^2} (\ell \cdot \ell_1)^2 C_{\ell_1}^{\psi\psi} \right] \\ &\quad + \int \frac{d^2 \ell_1}{(2\pi)^2} (\ell_1 \cdot (\ell - \ell_1))^2 \left[ C_{\ell_1}^{\Theta\Theta} C_{|\ell - \ell_1|}^{\psi\psi} + C_{\ell_1}^{\Theta\psi} C_{|\ell - \ell_1|}^{\Theta\psi} \right]. \end{aligned} \quad (5)$$

The first term in Eq. (5) could be interpreted as a transfer of the angular power spectrum on scale  $\ell$  into lensing scale  $\ell_1$  while the second term is a consequence of the convolution of  $\Theta$  power spectra with the lensing power spectra. Our result is consistent with Hu (2000) except for an inclusion of the temperature anisotropy and lensing potential cross-correlation  $C_\ell^{\Theta\psi}$ .

### 2.2. Covariance Matrix and Fisher Analysis

In order to forecast the ability of a given survey to constrain cosmological parameters, we adopt the Fisher matrix formalism (Tegmark et al. 1997). The CMB lensing covariance matrices formalism is adapted from Benoit-Lévy et al. (2012) and the bandpower estimator from Smith et al. (2006). The bandpower estimator for lensed temperature anisotropies is given by

$$\Delta_i^{\tilde{\Theta}\tilde{\Theta}} = \frac{1}{4\pi f_{\text{sky}} \alpha_i} \int_{\ell \in i} d^2 \ell \left( \frac{\ell^2}{2\pi} \right) \tilde{\Theta}^*(\ell) \tilde{\Theta}(\ell), \quad (6)$$

where  $f_{\text{sky}}$  is the fraction of the sky covered by the survey.

$$\alpha_i = \int_{\ell \in i} d^2 \ell, \quad (7)$$

is the integrated  $\ell$ -space area of the  $i$ th band power. In this article, we only consider the temperature anisotropy. From the estimator in Eq. (6), the covariance matrix for temperature anisotropy autocorrelation is

$$\text{Cov}(\Delta^{\tilde{\Theta}\tilde{\Theta}}, \Delta^{\tilde{\Theta}\tilde{\Theta}})_{ij} = \langle \Delta_i^{\tilde{\Theta}\tilde{\Theta}} \Delta_j^{\tilde{\Theta}\tilde{\Theta}} \rangle - \langle \Delta_i^{\tilde{\Theta}\tilde{\Theta}} \rangle \langle \Delta_j^{\tilde{\Theta}\tilde{\Theta}} \rangle, \quad (8)$$

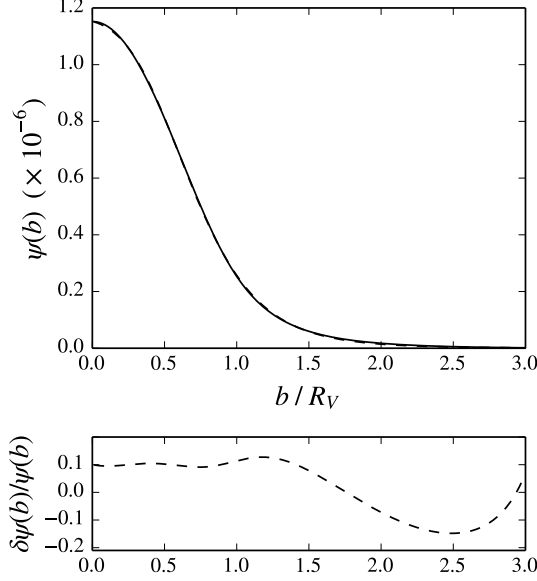


**Figure 2.** (top panel) The void lensing potential for  $R_V = 30.0 \text{ Mpc } h^{-1}$  at  $z = 0.5$  (solid) and the analytical fitting function Eq. (15) (dashed). (bottom panel) The fractional difference between the analytical fitting function and the lensing potential calculated numerically.

The indices  $i, j$  refer to bins in  $\ell$ -space. The full expression for  $\text{Cov}(\Delta^{\tilde{\Theta}\tilde{\Theta}}, \Delta^{\tilde{\Theta}\tilde{\Theta}})_{ij}$  is given in appendix A. We assume no cross-correlation between  $\Theta$  and  $\psi$  for voids. In term of the covariance matrix, the Fisher matrix is given by

$$F_{\alpha\beta} = \left( \frac{\partial}{\partial p_\alpha} \langle \Delta^{\tilde{\Theta}\tilde{\Theta}} \rangle \right)^T \left( \text{Cov}(\Delta^{\tilde{\Theta}\tilde{\Theta}}, \Delta^{\tilde{\Theta}\tilde{\Theta}}) \right)^{-1} \left( \frac{\partial}{\partial p_\beta} \langle \Delta^{\tilde{\Theta}\tilde{\Theta}} \rangle \right), \quad (9)$$

where  $p_\alpha$  and  $p_\beta$  are cosmological parameters on which the bandpower depends.  $\partial \langle \Delta^{\tilde{\Theta}\tilde{\Theta}} \rangle / \partial p_\alpha$  is a column vector of the partial derivative of  $\langle \Delta^{\tilde{\Theta}\tilde{\Theta}} \rangle$  with respect to the parameter  $p_\alpha$ . To simulate the instrumental noise, we add to the angular power spectra an assumed Gaussian noise for a PLANCK-like CMB survey<sup>9</sup> as explained in details in Chantavat et al. (2011).

### 3. METHODS

We now forecast the sensitivity of CMB lensing of voids on the temperature angular power spectrum of the CMB  $C_\ell$  on the surveys.

#### 3.1. Void Model

For most voids, the underdense central region is surrounded by an external over dense region called a *compensation*. The recent simulations of Hamaus et al. (2014b) have shown that the radial profile of *averaged* voids is spherically symmetric and is well fitted empirically by

$$\rho_V(r)/\bar{\rho}_M = 1 + \delta_c \frac{1 - (r/R_S)^\alpha}{1 + (r/R_V)^\beta}, \quad (10)$$

where  $\bar{\rho}_M$  is the mean cosmic matter density and  $R_V$  are the characteristic void radius.  $R_S$  is a scale radius where  $\rho_V = \bar{\rho}_M$ . We shall take the parameters as  $R_S/R_V = 0.93$ ,  $\alpha = 2.13$ ,  $\beta = 9.24$  and  $\delta_c = -0.85$  for  $R_V$  within  $20 - 50 \text{ Mpc } h^{-1}$

<sup>9</sup> See <http://www.rssd.esa.int/index.php?project=planck> for PLANCK specifications.

(Hamaus et al. 2014b). The choice of parameters are made such that the voids are well compensated. Even though voids, in general, do not have a spherical shape as in the stacked void profile, we shall take the average over many voids with different ellipticities and orientations as our approximation (Pisani et al. 2014).

For a weak gravitational field and a perfect fluid assumption, the distortion of spacetime is caused by the Newtonian gravitational potential  $\Psi_N$  which obeys the Poisson equation,

$$\nabla^2 \Psi_N = 4\pi G \bar{\rho}_M (1+z) D_+(z) \delta_M(z) = 0, \quad (11)$$

where  $\nabla$  is the comoving gradient operator.  $D_+(z)$  is the linear growth function normalised to unity at the present epoch and  $z$  is the redshift. The gravitational lensing potential  $\psi(\hat{n})$  is given by

$$\psi(\hat{n}) = -\frac{2}{c^2} \int d\chi \nabla_\perp \Psi_N(\chi \hat{n}), \quad (12)$$

where  $\chi$  is the comoving distance to the lensing source.  $\nabla_\perp$  is the transverse derivative. The integral is performed along the line of sight. Similarly, in term of angular separation  $\theta$ ,

$$\psi(\theta) = \int d^2 \hat{n} \left[ \sum_i^{N_V} \delta_D^2(\hat{n} - \hat{n}_i) \psi_i(\hat{n}_i; R_{V,i}, z_i) \right], \quad (13)$$

where  $N_V$  is the number of voids.  $\hat{n}_i$ 's are position of voids in the sky. The Fourier transform of the lensing potential into  $\ell$ -space is given by

$$\psi(\ell; R_V, z) = \int d^2 \theta \psi(\theta; R_V, z) \exp(-i\ell \cdot \theta). \quad (14)$$

We would advise the reader Amendola et al. (1999) on detailed calculation of the lensing potential from the Newtonian gravitational potential. Figure. 1 shows the lensing potentials of voids and their corresponding angular power spectra. The lensing potential in real space with voids as a function of the impact parameter  $\mathbf{b} \equiv D_K \theta$ , where  $D_K$  is the comoving angular diameter distance, is well approximated by the function

$$\psi(b; R_V, z) = S(R_V, z) \times \tilde{\psi}(b/R_V), \quad (15)$$

where  $\tilde{\psi}(x)$  is the scale-invariant lensing potential and  $S(R_V, z)$  is the lensing potential scaling factor.

$$\tilde{\psi}(x) = \psi_0 \exp(\Gamma_0 x^{\gamma_0}) \times (1.0 + x^{\gamma_1})^{\gamma_2}, \quad (16)$$

where  $\psi_0 = 9.06 \times 10^{-2} \text{ Mpc}^2 h^{-2}$ ,  $\gamma_0 = 1.29$ ,  $\gamma_1 = 2.86$ ,  $\gamma_2 = -1.72$ , and  $\Gamma_0 = -0.31$ .

$$S(R_V, z) = \frac{16\pi G}{c^2} \Omega_M \bar{\rho}_c \left( \frac{R_V}{\text{Mpc } h^{-1}} \right)^3 \frac{(1+z)^3 D_+(z)}{(D_K(z)/\text{Mpc } h^{-1})}, \quad (17)$$

where  $\bar{\rho}_c$  is the critical density at the present epoch. Our fitting function for the lensing potential is accurate within  $\sim 10\%$  over the range well within  $3R_V$  (See Figure. 2).

#### 3.2. Void Distribution

In order to give an estimate of the void distribution as a function of radius along the line of sight, the number density of voids is needed. As of the time of writing this paper, theoretical and empirical predictions of the number function are not well understood and still a matter of debate (Jennings et al. 2013; Sheth & van de Weygaert 2004; Sutter et al. 2014c). However, for our forecast on CMB lensing signal with voids

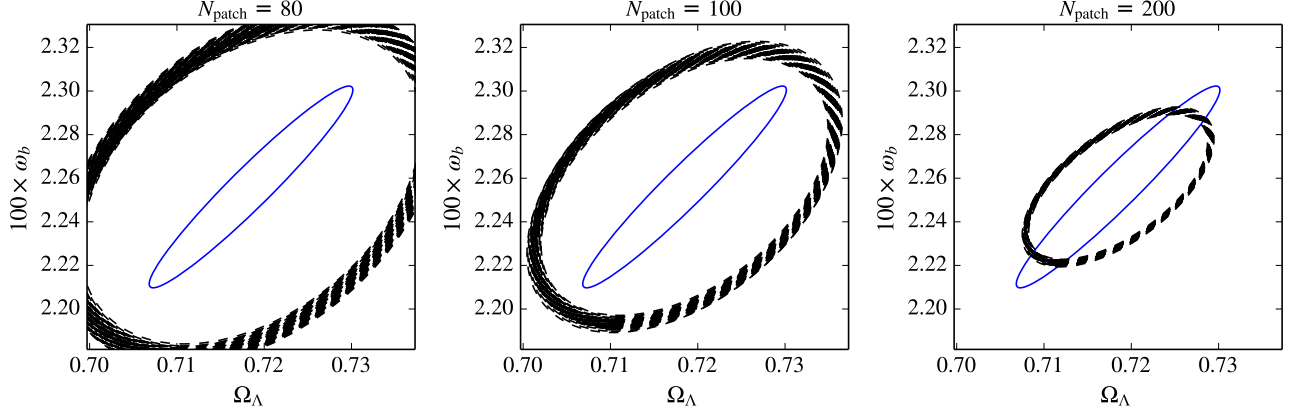


**Figure 3.** 95% CL for  $100 \times \omega_b$  and  $\Omega_\Lambda$  for  $N_V = 10$  along  $N_{\text{patch}}$  lines of sight with for full-sky PLANCK alone (solid) and multiple realisations of void populations (dashed). The scatter on constraints with different realisations is due to the sensitivity of the lensing potential with  $R_V$ .

we assume the void number function for a EUCLID-like mission based on [Sheth & van de Weygaert \(2004\)](#)

$$n_V(M) = \frac{\bar{\rho}_M}{M^2} \nu f(\nu) \frac{d \ln \nu}{d \ln M}, \quad (18)$$

where  $M$  is the void mass and  $\nu = \delta_v^2 / \sigma^2(M)$  with  $\delta_v$  being the critical under density for void and  $\sigma^2(M)$  is the variance of the density field.

$$\nu f(\nu) = \sqrt{\frac{\nu}{2\pi}} \exp\left(-\frac{\nu}{2}\right) \exp\left(-\frac{|\delta_c|}{\delta_v} \frac{\mathcal{D}^2}{4\nu} - 2\frac{\mathcal{D}^4}{\nu^2}\right), \quad (19)$$

where  $\mathcal{D} \equiv |\delta_v|/(\delta_c + |\delta_v|)$  and  $\delta_c = 1.686$ . We take  $\delta_v = -0.43$  from the HOD dense simulation in [Sutter et al. \(2014b\)](#). The radius distribution of voids in 1D space will be  $\sim n_V(R_V) D_K(z)^2 \times 1.0^\circ \times 1.0^\circ$  for a squared degree patch where  $R_V = 1.7 \times (3M/4\pi\bar{\rho}_M)^{1/3}$ . We shall also assume no redshift evolution of voids and take the redshift distribution as uniformly distributed within  $z = 0.0 - 1.0$ . The uniformity of void distribution with redshift is justified by the small dependence in redshift of [Lavaux & Wandelt \(2012\)](#)'s number function and little void evolution up to  $z = 1$  in the simulation by [Hamaus et al. \(2014a\)](#). At this stage we are not considering several practical difficulties which may complicate the recognition of voids in the surveys and assume that the surveys can identify voids down to characteristic size of  $R_V \sim 20 \text{ Mpc } h^{-1}$  for our fiducial surveys within the redshift range. We select voids of  $R_V > 20 \text{ Mpc } h^{-1}$  as indicated in [Hamaus et al. \(2014a\)](#), a transition radius from overcompensated to undercompensated voids. The undercompensated voids tends to inhibit in the underdense region of the universe where our lines of sight are chosen. The determination of void radius is subjected to the uncertainty in mapping the galaxies to the underlying dark matter ([Sutter et al. 2014a](#)). In this analysis, we assume 10% statistical uncertainty in  $R_V$  measurement which will be marginalised over the cosmological parameters.

### 3.3. Void Misalignment

We shall model how the centre of the voids are misaligned along the line of sight by allowing the centres of void to be offset uniformly within a field of view in Eq. (13). As small voids are commonly found in overdensed structure, larger voids are more abundant when we select patches of the sky which are free of clusters from low- $z$  cluster surveys. Given a pre-selected patch of the sky with no clusters found in low- $z$  sur-

veys, the chance of encountering sizeable clusters to the field of view at higher redshift is assumed negligible. The distribution of voids is assumed Poissonian; therefore the lensing effect of voids whose centre are out of the field of view are averaged out. In addition, we assume a nominal  $f_{\text{patch}}$  of  $1.0^\circ \times 1.0^\circ$  such that voids with  $R_V > 20 \text{ Mpc } h^{-1}$  could be well observed within the patch from  $z = 0.0 - 1.0$ .

We can express the lensing potential of voids as

$$\psi_{\text{total}}(\theta) = \sum_j^{N_V} \psi_j(\theta - \theta_j), \quad (20)$$

where  $\psi_j(\theta)$  is the lensing potential of  $j$ th void and  $\theta_j$  is the centre of the  $j$ th void from the common centre. The contribution to the angular power spectrum due to lensing effect of voids is given by

$$C_{\ell, \text{total}}^{\psi\psi} = \sum_j^{N_V} C_{\ell, j}^{\psi\psi} + 2 \sum_{j < k}^{N_V} J_0(\ell \Delta\theta_{jk}) \langle \psi_j(\ell) \psi_k^*(\ell) \rangle, \quad (21)$$

where  $\Delta\theta_{jk} \equiv \theta_j - \theta_k$  and  $J_n(x)$  is the Bessel function of the first kind. The first term is the correlation from the same void and the second term is the correlation due to different voids. The detail derivation for Eq. (21) is given in appendix B.

To summarise our method, we shall proceed as follow:

- Generate 100 realisations of voids distributed along a line of sight given in terms of  $R_V$  and  $z$  for  $N_V = 10$  within a sky patch of  $1.0^\circ \times 1.0^\circ$  for  $N_{\text{patch}}$  patches of the sky per realisation taking the misalignment into account.
- The lensing potential in Eq. (14) is calculated from the void profile (Eq. (10)) for each void in a given realisation. The resulting void lensing potentials in a line-of-sight are combined in Eq. (21) for  $C_{\ell, \text{total}}^{\psi\psi}$  in the line of sight.
- Calculate the covariance matrices (Eq. (A1)) and the Fisher matrices (Eq. (9)) and get the parameter constraints with  $R_V$  as a nuisance parameter to be marginalised with 10% prior on  $R_V$ .



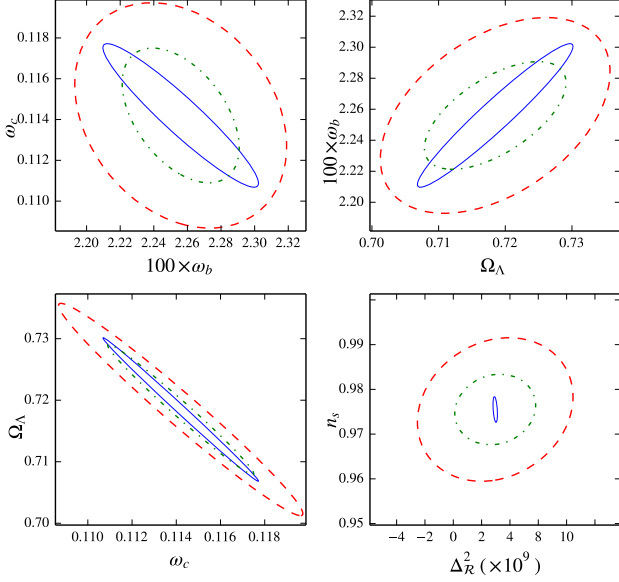


**Figure 4.** 95% CL constraints on some of the cosmological parameter pairs:  $100 \omega_b$  &  $\omega_c$  (top-left),  $\Omega_\Lambda$  &  $100 \omega_b$  (top-right),  $\omega_c$  &  $\Omega_\Lambda$  (bottom-left) and  $\Delta_R^2$  &  $n_s$  (bottom-right) for full-sky PLANCK (solid), voids with  $N_{\text{patch}} = 100$  (dashed) and  $N_{\text{patch}} = 200$  (dot-dashed).

#### 4. RESULTS

The assumed number function gives an the mean radius of  $\bar{R}_V \approx 23.2 \text{ Mpc } h^{-1}$  in a low density part of the universe. In order to describe our ignorance in the number of patches that contains  $\approx 10$  voids and with negligible effect from clusters, we shall include  $N_{\text{patch}}$ , the number of such patches of the sky, as an independent parameter. The degeneracy between  $N_V$  and  $N_{\text{patch}}$  is obvious; however, in this article, we shall not take this additional degeneracy into account by fixing  $N_V = 10$  and investigate how the constraints could be improved with varying  $N_{\text{patch}}$ .

As an illustrative demonstration of the importance of the number of independent patches on cosmological parameter constraints from CMB lensing with voids, we shall take the  $100 \times \omega_b$  &  $\Omega_\Lambda$  pair as an example shown in Figure. 3. From the figure, the constraints vary significantly from one realisation to another due to the sensitivity of the lensing potential with  $R_V$  (See the right panel of Figure. 1). However, we have found that the constraints significantly improve with increasing  $N_{\text{patch}}$  and the scatter in size of the ellipses reduces as one would expect with many realizations. The constraints become competitive with PLANCK with  $N_{\text{patch}} \gtrsim 100$ . The full parameters constraint are shown in Table 1 where we choose the median of the ellipses as a representation of the realisations for  $N_{\text{patch}} = 80, 100, 200$ . Some of the interesting pairs of cosmological parameters are shown in Figure. 4 for  $N_{\text{patch}} = 100$  and  $200$ .

#### 5. DISCUSSIONS AND CONCLUSIONS

The main advantage of CMB lensing by voids arises from the fact that  $C_\ell^{\psi\psi}$  for voids scales approximately as  $\sim N_V^2$  along the line of sight. The scaling relation of void lensing power spectra comes from the linearity of the void lensing potential (See Eq. (20)). Hence, the void power spectra is enhanced over the intrinsic CMB power spectra by  $\sim N_V^2$ . However, the improvement on constraints cannot be infinite due to 1) the cosmic variance; 2) the limitation on the number of voids

available; 3) the scatter in the void profile. In this article, only 1) and 2) are considered. Another advantage is the sensitivity of  $C_\ell^{\psi\psi}$  with  $R_V$  (See Figure. 1). This implies that better constraints could be achieved with larger voids with the same number of voids and patches. However, the chance of spoiling the lensing effect by SZ effects of intervening clusters of galaxies is higher due to larger angular extent which effectively reduces the number of  $N_{\text{patch}}$ . The impact from SZ contamination is expected to be more important than the lensing caused by clusters: the typical angular extension,  $\theta_{500}$ , of SZ temperature profile is a few  $10'$  to  $100'$  (see e.g. Whitbourn et al. 2014; Planck Collaboration 2013c).

We have shown that with pre-selected parts of the sky where no clusters are found, or small enough to be of no significant effect, void lensing could potentially provided cosmological constraints at a level competitive with PLANCK alone. The assumption of finding sizeable cluster at higher redshift is crucial in the analysis. We use Jenkins et al. (2001) mass function and Cooray & Sheth (2002) to calculate a cluster of size  $> 20 \text{ Mpc } h^{-1}$  and found that the probability is  $\lesssim 10^{-5}$  which is negligible. In addition, we assume that, regarding to the angular size of the patch at a given redshift, the lensing effect of intervening galaxies are negligible. The validity of our results relies on the search for such  $1.0^\circ \times 1.0^\circ$  patches of the sky.

For  $N_{\text{patch}} \gtrsim 100$ , the overall constraining power is better than PLANCK for the density parameter ( $\omega_b$ ,  $\omega_c$  and  $\Omega_\Lambda$ ) but not with  $n_s$ ,  $\Delta_R^2$  and  $\tau$ . This is due to the fact that the dependence of the growth function on these parameters is weak and an additional information of large-scale structure at different redshifts does not improve the constraints on those parameters. Even though our void profile does not have an explicit dependence on  $\omega_b$ , the improvement on  $\omega_b$  is due to the fact that the lensed power spectra with voids are convolution functions of the intrinsic CMB power spectra that depend on  $\omega_b$ . The general correlation directions does not significantly differ from PLANCK due to the weaker void signal in comparison to the intrinsic CMB angular power spectrum.

The other secondary effect besides lensing are notably the Sunyaev-Zel'dovich effect (Zel'dovich 1968) and the Rees-Sciama (RS) effect (Rees & Sciama 1968). The SZ effect is expected not to have a sizeable contribution in an underdense region (Birkinshaw 1999). One would expect that there should be no SZ effect from voids at all as there should be no significant amount of gas. The RS effect, however, may have a significant effect for very large voids,  $|\delta T^{\text{RS}}/T| \propto R_V^\beta$  where  $\beta \approx 2.5 - 3.0$ . For a single void with  $R_{V, \text{eff}} = \bar{R}_V \approx 23.2 \text{ Mpc } h^{-1}$ , the predicted  $\ell(\ell+1)C_\ell^{\psi\psi}/2\pi \approx 0.1 \mu\text{K}^2$  at  $\ell \approx 100 - 200$ . For a one square-degree patch with 10 of those voids in the sight line, lensing contribution becomes  $\ell(\ell+1)C_\ell^{\psi\psi}/2\pi \approx 600 \mu\text{K}^2$ . A full-sky ray-tracing analysis by Cai et al. (2010) estimated the RS contribution to the CMB anisotropy  $\ell(\ell+1)C_\ell^{\text{RS}}/2\pi \approx 0.1 \mu\text{K}^2$  at the similar multipoles for redshift slice  $0.17 < z < 0.57$  for both voids and clusters. In this work, we therefore neglect the RS effect for the aforementioned reasons. A full ray-tracing analysis of weak lensing and other secondary anisotropies from voids will be the subject of our future investigation.

We would like to thank Sirichai Chongchitnan, Nico Hamaus for useful comments; Khamphree Karwan for his generous provision of computing facilities in numerically intensive parts of our calculation. TC acknowledges the support

	$100 \times \sigma_{\omega_b}$	$\sigma_{\omega_c}$	$\sigma_{\Omega_\Lambda}$	$\sigma_{\Delta_{\mathcal{R}}^2} \times 10^9$	$\sigma_{n_s}$	$\sigma_\tau$
PLANCK	0.0586	0.00667	0.0205	0.396	0.00479	0.0815
$N_{\text{patch}} = 100$	0.0505	0.00445	0.0139	11.054	0.02583	2.4947
$N_{\text{patch}} = 200$	0.0280	0.00266	0.00854	5.7462	0.01268	1.3039
$N_{\text{patch}} = 400$	0.0165	0.00167	0.00547	2.9800	0.00631	0.6776

**Table 1**

68% CL parameter constraints on the fiducial cosmological parameters for PLANCK, and voids with  $N_{\text{patch}} = 100, 200, 400$ .

from the National Astronomical Research Institute of Thailand (NARIT) and Naresuan University grant R2555C018. This work is supported by NARIT research grant and its High Performance Computer facility.

## REFERENCES

Aghanim, N., Majumdar, S., & Silk, J. 2008, Reports on Progress in Physics, 71, 066902  
 Amendola, L., Frieman, J. A., & Waga, I. 1999, MNRAS, 309, 465  
 Bartelmann, M. & Schneider, P. 2001, Phys. Rep., 340, 291  
 Benoit-Lévy, A., Smith, K. M., & Hu, W. 2012, Phys. Rev. D, 86, 123008  
 BigBOSS Collaboration 2009, arXiv:0904.0468  
 Birkinshaw, M. 1999, Phys. Rep., 310, 97  
 Biswas, R., Alizadeh, E., & Wandelt, B. D. 2010, Phys. Rev. D, 82, 023002  
 Blanchard, A. & Schneider, J. 1987, A&A, 184, 1  
 Bos, E. G. P. et al. 2012, MNRAS, 426, 440  
 Boylan-Kolchin, M. et al. 2009, MNRAS, 398, 1150  
 Cai, Y.-C., Cole, S., Jenkins, A., & Frenk, C. S. 2010, MNRAS, 407, 201  
 Cai, Y.-C. et al. 2014, ApJ, 786, 110  
 Carroll, S. M., Press, W. H., & Turner, E. L. 1992, ARA&A, 30, 499  
 Chantavat, T., Gordon, C., & Silk, J. 2011, Phys. Rev. D, 83, 103501  
 Cooray, M. & Sheth, P. 2002, Phys. Rep., 372, 1  
 DES Collaboration 2006, astro-ph/0609591  
 Hamaus, N. et al. 2014a, Phys. Rev. Lett., 112, 041304  
 Hamaus, N. et al. 2014b, Phys. Rev. Lett., 112, 251302  
 Higuchi, Y., Oguri, M., & Hamana, T. 2013, MNRAS, 432, 1021  
 Hinshaw, G. et al. 2013, ApJS, 208, 19

Hu, W. 2000, Phys. Rev. D, 62, 043007  
 Ilić, S., Langer, M., & Douspis, M. 2013, A&A, 556, A51  
 Jenkins, A. et al. 2001, MNRAS, 321, 372  
 Jennings, E., Li, Y., & Hu, W. 2013, MNRAS, 434, 2164  
 Krause, E. et al. 2013, ApJL, 762, L20  
 Laureijs, R. et al. 2011, arXiv:1110.3193  
 Lavaux, G. & Wandelt, B. D. 2012, ApJ, 754, 109  
 Lewis, A. & Challinor, A. 2006, Phys. Rep., 429, 1  
 Lewis, A., Challinor, A., & Lasenby, A. 2000, ApJ, 538, 473  
 LSST Science Collaboration 2009, arXiv:0912.0201  
 Melchior, P. et al. 2014, MNRAS, 440, 2922  
 Pan, D. C. et al. 2012, MNRAS, 421, 926  
 Pisani, A. et al. 2014, MNRAS, 443, 3238  
 Planck Collaboration 2013a, arXiv:1303.5076  
 —. 2013b, arXiv:1303.5079  
 —. 2013c, arXiv:1303.5089  
 Rees, M. J. & Sciama, D. W. 1968, Nature, 217, 511  
 Sheth, R. K. & van de Weygaert, R. 2004, MNRAS, 350, 517  
 Smith, K. M., Hu, W., & Kaplinghat, M. 2006, Phys. Rev. D, 74, 123002  
 Sutter, P. M. et al. 2012a, ApJ, 761, 44  
 —. 2012b, ApJ, 761, 187  
 Sutter, P. M. et al. 2014a, MNRAS, 438, 3177  
 —. 2014b, MNRAS, 442, 462  
 —. 2014c, MNRAS, 442, 3127  
 Tegmark, M., Taylor, A. N., & Heavens, A. F. 1997, ApJ, 480, 22  
 Whitbourn, J. R., Shanks, T., & Sawangwit, U. 2014, MNRAS, 437, 622  
 Zel'dovich, Y. B. 1968, Soviet Physics Uspekhi, 11, 381

## APPENDIX

### A. COVARIANCE MATRIX FOR CMB LENSING

Following Smith et al. (2006), we obtain the expression for the covariance matrix for CMB Lensing,

$$\text{Cov}(\Delta^{\tilde{\Theta}\tilde{\Theta}}, \Delta^{\tilde{\Theta}\tilde{\Theta}})_{ij} = \langle \Delta_i^{\tilde{\Theta}\tilde{\Theta}} \Delta_j^{\tilde{\Theta}\tilde{\Theta}} \rangle - \langle \Delta_i^{\tilde{\Theta}\tilde{\Theta}} \rangle \langle \Delta_j^{\tilde{\Theta}\tilde{\Theta}} \rangle, \quad (A1)$$

$$= \mathcal{G}_i \delta_{ij} + \mathcal{H}_i \delta_{ij} + \mathcal{I}_{ij} + \mathcal{J}_{ij},$$

where the indices  $i, j$  refer to bins in  $\ell$ -space and  $\delta_{ij}$  is the Kronecker's delta.  $\mathcal{G}_i$  is the Gaussian term and the other terms are the non-Gaussian parts of the covariance matrix. The Gaussian part is given by

$$\mathcal{G}_i = \frac{2(2\pi)^2}{4\pi f_{\text{sky}} \alpha_i^2} \int_{\ell \in i} d^2 \ell \left( \frac{\ell^2}{2\pi} \right)^2 C_{\ell}^{\Theta\Theta} C_{\ell}^{\Theta\Theta}. \quad (A2)$$

The other terms are given by

$$\mathcal{H}_i = \frac{4}{4\pi f_{\text{sky}} \alpha_i^2} \int_{\ell \in i} d^2 \ell \ell^4 \int \frac{d^2 \ell_1}{(2\pi)^2} \left[ C_{\ell}^{\Theta\Theta} (C_{\ell_1}^{\Theta\Theta} C_{|\ell-\ell_1|}^{\psi\psi} + C_{\ell_1}^{\Theta\psi} C_{|\ell-\ell_1|}^{\Theta\psi}) ((\ell - \ell_1) \cdot \ell_1)^2 - C_{\ell}^{\Theta\Theta} C_{\ell}^{\Theta\Theta} C_{\ell_1}^{\psi\psi} (\ell \cdot \ell_1)^2 \right], \quad (A3)$$

$$\mathcal{I}_{ij} = -\frac{2}{4\pi f_{\text{sky}} \alpha_i \alpha_j} \int_{\ell \in i} d^2 \ell \int_{\ell' \in j} d^2 \ell' \left( \frac{\ell^2}{2\pi} \right) \left( \frac{\ell'^2}{2\pi} \right) \times (C_{\ell}^{\Theta\Theta} C_{\ell'}^{\Theta\psi} C_{\ell'}^{\Theta\psi} + C_{\ell'}^{\Theta\Theta} C_{\ell}^{\Theta\psi} C_{\ell}^{\Theta\psi}) (\ell \cdot \ell')^2, \quad (A4)$$

$$\mathcal{J}_{ij} = \frac{1}{4\pi f_{\text{sky}} \alpha_i \alpha_j} \int_{\ell \in i} d^2 \ell \int_{\ell' \in j} d^2 \ell' \left( \frac{\ell^2}{2\pi} \right) \left( \frac{\ell'^2}{2\pi} \right) \times \left( 2\alpha_+ (\ell, \ell') \mathcal{M}_+ (\ell, \ell') \mathcal{M}_+ (\ell', \ell) + 2\alpha_- (\ell, \ell') \mathcal{M}_- (\ell, \ell') \mathcal{M}_- (\ell', \ell) \right. \\ \left. + \beta_+ (\ell, \ell') \mathcal{M}_+ (\ell, \ell')^2 + \beta_+ (\ell', \ell) \mathcal{M}_+ (\ell', \ell)^2 + \beta_- (\ell, \ell') \mathcal{M}_- (\ell, \ell')^2 + \beta_- (\ell', \ell) \mathcal{M}_- (\ell', \ell)^2 \right), \quad (A5)$$

where

$$\mathcal{M}_{\pm}(\ell, \ell') = (\ell \pm \ell') \cdot \ell, \quad (\text{A6})$$

$$\alpha_{\pm}(\ell, \ell') = C_{\ell}^{\Theta\Theta} C_{\ell'}^{\Theta\Theta} C_{|\ell \pm \ell'|}^{\psi\psi} + C_{\ell}^{\Theta\Theta} C_{\ell'}^{\Theta\psi} C_{|\ell \pm \ell'|}^{\Theta\psi} + C_{\ell'}^{\Theta\Theta} C_{\ell}^{\Theta\psi} C_{|\ell \pm \ell'|}^{\Theta\psi} + C_{\ell'}^{\Theta\psi} C_{\ell}^{\Theta\psi} C_{|\ell \pm \ell'|}^{\Theta\Theta}, \quad (\text{A7})$$

$$\beta_{\pm}(\ell, \ell') = C_{\ell}^{\Theta\Theta} C_{\ell'}^{\Theta\Theta} C_{|\ell \pm \ell'|}^{\psi\psi} + C_{\ell}^{\Theta\Theta} C_{\ell'}^{\Theta\psi} C_{|\ell \pm \ell'|}^{\Theta\psi} + C_{\ell'}^{\Theta\Theta} C_{\ell}^{\Theta\psi} C_{|\ell \pm \ell'|}^{\Theta\psi} + C_{\ell'}^{\Theta\psi} C_{\ell}^{\Theta\psi} C_{|\ell \pm \ell'|}^{\Theta\Theta}. \quad (\text{A8})$$

Our result is consistent with [Smith et al. \(2006\)](#) except for inclusion of the temperature anisotropy and lensing potential cross-correlation function. In addition, we found correction terms due to the second order expansion in Eq. (3).

#### B. ANGULAR POWER SPECTRUM FOR MULTIPLY NEARLY-ALIGNED LENSING SOURCES

Suppose that we have  $N$  number of lensing sources slightly misaligned along a line of sight, we can write the total lensing potential as

$$\psi_{\text{total}}(\theta) = \psi_1(\theta - \theta_1) + \dots + \psi_N(\theta - \theta_N), \quad (\text{B1})$$

where  $\psi_j(\theta)$  is the lensing potential of  $j$ th lensing source and  $\theta_j$  is the centre of the  $j$ th source from the common centre. The Fourier transform of the whole system will be

$$\begin{aligned} \psi_{\text{total}}(\ell) &= \int d^2\theta \psi_{\text{total}}(\theta) \exp(-i\ell \cdot \theta), \\ &= \int d^2\theta \sum_j \psi_j(\theta - \theta_j) \exp(-i\ell \cdot \theta), \\ \psi_{\text{total}}(\ell) &= \sum_j \int d^2\theta \psi_j(\theta) \exp(-i\ell \cdot (\theta + \theta_j)). \end{aligned} \quad (\text{B2})$$

Since the angle  $(\ell \cdot \theta)$  and  $(\ell \cdot \theta_j)$  are independent (clearly shown if we express in Cartesian coordinates), hence

$$\begin{aligned} \psi_{\text{total}}(\ell) &= \sum_j \exp(-i\ell \cdot \theta_j) \int d^2\theta \psi_j(\theta) \exp(-i\ell \cdot \theta), \\ &= \sum_j \exp(-i\ell \cdot \theta_j) \psi_j(\ell). \end{aligned} \quad (\text{B3})$$

The angular correlation will be given by

$$\begin{aligned} C_{\ell, \text{total}}^{\psi\psi} &= \langle \psi_{\text{total}}(\ell) \psi_{\text{total}}^*(\ell) \rangle, \\ &= \left\langle \left( \sum_j \exp(-i\ell \cdot \theta_j) \psi_j(\ell) \right) \left( \sum_k \exp(i\ell \cdot \theta_k) \psi_k^*(\ell) \right) \right\rangle, \\ &= \sum_j C_{\ell, j}^{\psi\psi} + \sum_{j \neq k} \exp(-i\ell \cdot (\theta_j - \theta_k)) \langle \psi_j(\ell) \psi_k^*(\ell) \rangle, \\ C_{\ell, \text{total}}^{\psi\psi} &= \sum_j C_{\ell, j}^{\psi\psi} + \mathcal{D}, \end{aligned} \quad (\text{B4})$$

where

$$\mathcal{D} \equiv \sum_{j \neq k} \exp(-i\ell \cdot (\theta_j - \theta_k)) \langle \psi_j(\ell) \psi_k^*(\ell) \rangle, \quad (\text{B5})$$

is the small-scale correction due to the misalignment. Exploiting the symmetry of the system,

$$\langle \psi_j(\ell) \psi_k^*(\ell) \rangle = \langle \psi_k(\ell) \psi_j^*(\ell) \rangle. \quad (\text{B6})$$

Therefore,

$$\begin{aligned} \mathcal{D} &= \sum_{j \neq k} \exp(-i\ell \cdot (\theta_j - \theta_k)) \langle \psi_j(\ell) \psi_k^*(\ell) \rangle, \\ &= \sum_{j < k} \left( \exp(-i\ell \cdot \Delta\theta_{jk}) + \exp(i\ell \cdot \Delta\theta_{jk}) \right) \langle \psi_j(\ell) \psi_k^*(\ell) \rangle, \\ \mathcal{D} &= 2 \sum_{j < k} \cos(\ell \cdot \Delta\theta_{jk}) \langle \psi_j(\ell) \psi_k^*(\ell) \rangle, \end{aligned} \quad (\text{B7})$$

where  $\Delta\boldsymbol{\theta}_{jk} \equiv \boldsymbol{\theta}_j - \boldsymbol{\theta}_k$ . By performing an average over the angle  $\boldsymbol{\ell} \cdot \Delta\boldsymbol{\theta}_{jk}$  in Eq. (B7) and exploiting the relation

$$\frac{1}{2\pi} \int_0^{2\pi} d\phi \cos(x \cos \phi) = J_0(x), \quad (\text{B8})$$

where  $J_n(x)$  is the Bessel function of the first kind. Hence, the angular power spectrum of the system is given by

$$C_{\ell, \text{total}}^{\psi\psi} = \sum_j C_{\ell, j}^{\psi\psi} + 2 \sum_{j < k} J_0(\ell \Delta\theta_{jk}) \langle \psi_j(\boldsymbol{\ell}) \psi_k^*(\boldsymbol{\ell}) \rangle. \quad (\text{B9})$$